Journal of Physics: Condensed Matter

PAPER

Large anisotropy of magnetic damping in amorphous CoFeB films on GaAs(001)

To cite this article: Hongqing Tu *et al* 2020 *J. Phys.: Condens. Matter* **32** 335804

IOP Publishing Journal of Physics: Condensed Matter
J. Phys.: Condens. Matter **32** (2020) 335804 (7pp) https://doi.org/10.1088/1361-648X/ab8984

Large anisotropy of magnetic damping in amorphous CoFeB films on GaAs(001)

Hongqing Tu[1,2,7], Ji Wang[1,7], Zhaocong Huang[3], Ya Zhai[3], Zhendong Zhu[4], Zongzhi Zhang[4], Jiangtao Qu[5], Rongkun Zheng[5], Yuan Yuan[1], Ruobai Liu[1], Wei Zhang[1], Biao You[1,6] and Jun Du[1,6,8]

[1] National Laboratory of Solid State Microstructures and Department of Physics, Nanjing University, Nanjing 210093, People's Republic of China
[2] Department of Mathematics and Physics, Nanjing Institute of Technology, Nanjing 211167, People's Republic of China
[3] Department of Physics and Jiangsu Key Laboratory of Advanced Metallic Materials, Southeast University, Nanjing 211189, People's Republic of China
[4] Key Laboratory of Micro and Nano Photonic Structures (Ministry of Education), Department of Optical Science and Engineering, Shanghai Ultra-Precision Optical Manufacturing Engineering Center, Fudan University, Shanghai 200433, People's Republic of China
[5] School of Physics and the Australian Institute for Nanoscale Science and Technology, The University of Sydney, NSW 2006, Australia
[6] Collaborative Innovation Center of Advanced Microstructures, Nanjing 210093, People's Republic of China

E-mail: jdu@nju.edu.cn

Received 31 March 2020, revised 7 April 2020
Accepted for publication 15 April 2020
Published 20 May 2020

Abstract

Amorphous CoFeB films grown on GaAs(001) substrates demonstrating significant in-plane uniaxial magnetic anisotropy were investigated by vector network analyzer ferromagnetic resonance. Distinct in-plane anisotropy of magnetic damping, with a largest maximum–minimum damping ratio of about 109%, was observed via analyzing the frequency dependence of linewidth in a linear manner. As the CoFeB film thickness increases from 3.5 nm to 30 nm, the amorphous structure for all the CoFeB films is maintained while the magnetic damping anisotropy decreases significantly. In order to reveal the inherent mechanism responsible for the anisotropic magnetic damping, studies on time-resolved magneto-optical Kerr effect and high resolution transmission electron microscopy were performed. Those results indicate that the in-plane angular dependent anisotropic damping mainly originates from two-magnon scattering, while the Gilbert damping keeps almost unchanged.

Keywords: magnetic damping, two-magnon scattering, Gilbert damping, ferromagnetic resonance, amorphous film

S Supplementary material for this article is available online

(Some figures may appear in colour only in the online journal)

[7] These authors contributed equally.

[8] Author to whom any correspondence should be addressed.

1. Introduction

Magnetic damping governs the performance of spintronic devices including hard drives, magnetic random access memories, magnetic logic devices, and magnetic field sensors [1, 2]. In general, it is understood that the magnetic damping reflects energy and angular momentum dissipation from the excited uniform spin motions directly to lattice or to spin waves ($k \neq 0$) initially and to lattice finally [3]. The former is the intrinsic damping specified by the LLG equation, which can be expressed by [4]

$$\frac{\mathrm{d}\mathbf{m}}{\mathrm{d}t} = -\gamma\mu_0\mathbf{m} \times \mathbf{H}_{\mathrm{eff}} + \alpha\mathbf{m} \times \frac{\mathrm{d}\mathbf{m}}{\mathrm{d}t}, \qquad (1)$$

where $\mathbf{m}$ is the unit magnetization vector, $\mathbf{H}_{\mathrm{eff}}$ is the effective magnetic field, γ is the gyromagnetic ratio described by $\gamma = \mathrm{g}\mu_{\mathrm{B}}/h$, and α is the Gilbert damping value. The latter refers to spin-wave-dominated damping mechanism, such as the commonly known two-magnon scattering (TMS), which is an extrinsic contribution to magnetic damping and provides a pathway for transferring energy from the uniform spin motions to the short-wavelength spin waves and then to the lattice [5–7]. Unambiguously, both the intrinsic and extrinsic mechanisms can cause energy dissipation of the magnetic precession and determine the efficiency and power consumption of the spintronic devices [8, 9]. Therefore, it is of great importance to manipulate magnetic damping within the same device, although little progress has been achieved so far.

Utilization of spin torque is a method to manipulate the magnetic damping [10–13], however, the requirement of large current density restricts its practical application. Alternatively, if the magnetic damping has prominent anisotropy, it can be tuned easily by rotating the magnetization orientation within the same device. Unfortunately, although several theoretical works predicted that Gilbert damping could be anisotropic in some single-crystalline ferromagnets, such as Fe, Co and Ni [14], the effect of experimental observation was too weak to be convincing. Until very recently, several exciting findings aroused people's interests. L Chen *et al* reported that the Gilbert damping is anisotropic in ultrathin single-crystalline Fe film deposited on GaAs(001) substrate and attributed this to the anisotropic density of state at the Fermi level [15]. Soon after, Y Li *et al* demonstrated a giant Gilbert damping anisotropy of 400% in epitaxial CoFe thin films deposited on MgO(100) substrate, which is due to the variation of the spin–orbit coupling for different magnetization orientations [16]. These two studies both excluded the TMS contributions. The anisotropy of magnetic damping has been also observed in some epitaxial magnetic alloy films, such as Co_2FeAl [17–19], Co_2FeSi [20], Co_2MnSi [21] and FeGa [22], although whether the origin of the damping anisotropy is intrinsic or extrinsic remains controversial.

Up to now, magnetic anisotropic damping has been all found in single-crystalline or high textured polycrystalline magnetic thin films, which normally shows fourfold magnetocrystalline anisotropy (MCA) and twofold uniaxial magnetic anisotropy (UMA) simultaneously. No efforts were undertaken on the anisotropic damping for amorphous ferromagnetic thin films, which may rule out the influence of MCA and meantime demonstrate a pure twofold UMA. For example, very thin CoFeB film deposited on GaAs substrate could exhibit a pure and significant in-plane UMA and its anisotropic field could be even larger than 300 Oe [23–27]. In this work, we have investigated the in-plane magnetic damping in the amorphous CoFeB films on GaAs(001) substrates by vector network analyzer ferromagnetic resonance (VNA-FMR) in combination with time-resolved magneto-optical Kerr effect (TRMOKE) techniques. Interestingly, the effective magnetic damping along the UMA hard axis (HA) is obviously larger than that along the easy axis (EA), and the inherent mechanism responsible for the anisotropic magnetic damping is addressed.

2. Experimental

The commercial GaAs(001) wafers were used with the major-flat direction along [110] and the secondary-flat direction along [1–10]. The GaAs wafer is *n*-type with very light doping (Si-doped, 10^{16}–10^{17} cm^{-3}). These wafers were diced into about 4 mm × 4 mm pieces as substrates. Before deposition, the surface of the substrate needs to be etched/cleaned by proper procedures as reported previously [25, 26]. At room temperature, four CoFeB films with different thicknesses, i.e. 3.5 nm (A1), 10 nm (A2), 20 nm (A3) and 30 nm (A4) were deposited on GaAs(001) substrates by dc magnetron sputtering at normal incidence from a $Co_{56}Fe_{24}B_{20}$ alloy target. It needs to be emphasized that no bias magnetic field was applied and the substrates were held still without self-rotating or sweeping during deposition. Sample A2 is chosen as a representative and will be discussed in detail in the following. A Ta film of 2 nm was deposited as capping layer to prevent the CoFeB film from oxidation. The base pressure was lower than 8.0×10^{-6} Pa and the Ar pressure was kept at 0.3 Pa during film deposition.

The crystalline structures of the samples were characterized by x-ray diffraction (XRD, Bruker D8-Advance) with Cu K_α radiation. In order to know the microstructure of the film, especially for the locations near the film-substrate interface, cross-sectional high-resolution transmission electron microscopy (TEM, JEOL 2200FS) characterizations were performed. The in-plane magnetic hysteresis (M–H) loops were measured by a superconducting quantum interference device-vibrating sample magnetometer (SQUID-VSM, Quantum Design). To study the in-plane anisotropy of magnetic damping for the GaAs(001)/CoFeB films, a home-made VNA-FMR equipment was employed with its microwave frequency varied from 5 GHz to 18 GHz. A home-made pump-probe TRMOKE equipment was also used to characterize the magnetic damping.

3. Results and discussion

As shown in figure 1, the XRD patterns for all the four samples are much similar to that of pure GaAs(001) substrate and no obvious diffraction peaks for Fe, Co, FeCo and other alloys can be observed, indicating amorphous structures for all the CoFeB films with thickness varied from 3.5 nm to 30 nm. The

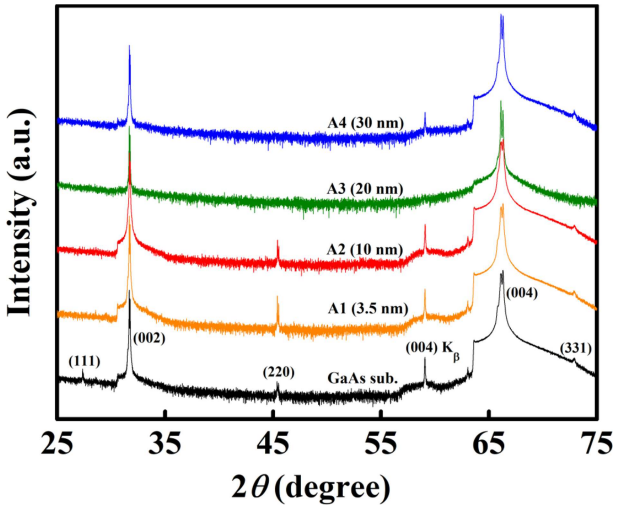

Figure 1. XRD patterns for all the CoFeB film samples and a pure GaAs(001) substrate.

geometry of FMR measurement is schematically displayed in figure 2(a). H and M denote the external magnetic field and the magnetization, respectively. The azimuthal angle of $H(M)$, i.e. φ_H (φ_M), denotes the angle rotating anticlockwise from [110] to the projection of $H(M)$. In the present experimental studies, since H is always applied in the film plane, $\theta_H = \theta_M = 0°$. The geometry of the TRMOKE measurement is exhibited in figure 2(b). While the azimuthal angle φ_H changes from 0° to 90°, the out-of-plane angle β_H, which denotes the angle rotated away from the film plane, is fixed at 19° during the measurement.

The experimental values of resonance field (H_r) and linewidth (ΔH, defined by the full width at half maximum of the FMR spectrum) can be obtained by fitting the FMR spectrum with both the symmetric and asymmetric parts [27]. The total free energy per unit volume can be written as

$$F = -HM_S[\sin\theta_M \sin\theta_H \cos(\varphi_H - \varphi_M) + \cos\theta_M \cos\theta_H] - \left(2\pi M_S^2 - K_P\right)\sin^2\theta_M - K_u \sin^2\theta_M \cos^2\varphi_M, \quad (2)$$

where the densities of Zeeman energy, effective demagnetized energy, and in-plane UMA energy are described in the first, second and third terms, respectively. The definition of θ_H (θ_M) can be referred in figure 2(a). M_s, K_P and K_u denote the saturate magnetization, out-of-plane and in-plane UMA energy constants, respectively. Since the magnetic field is always applied in the film plane, the precession frequency f at resonance and the equilibrium equation can be derived to be [4, 28]

$$f = \frac{\gamma}{2\pi}\sqrt{H_1 H_2} \quad (3)$$

$$H_r \sin(\varphi_H - \varphi_M) - \frac{1}{2}H_u \sin(2\varphi_M) = 0, \quad (4)$$

where $H_1 = H_r \cos(\varphi_H - \varphi_M) + 4\pi M_{eff} + H_u \cos^2\varphi_M$, $H_2 = H_r \cos(\varphi_H - \varphi_M) + H_u \cos(2\varphi_M)$, H_r is the resonance field; $4\pi M_{eff} = 4\pi M_S - H_P$, $H_u = 2K_u/M_S$, $H_P = 2K_P/M_S$. Therefore, H_u denotes the in-plane UMA field and will be discussed in detail in the following.

Figures 3(a) and (b) show the in-plane angular dependent H_r for sample A2 at f = 10 GHz and 13 GHz, respectively. By taking into account an in-plane UMA solely, the experimental H_r–φ_H results can be well fitted and H_u is calculated to be about 192 Oe. This result indicates that there exists a significant and pure in-plane UMA with the EA along [110] and the HA along [1–10]. Similar twofold symmetry of the azimuthal angular dependent H_r can also be observed at other frequencies, e.g. f = 8 GHz and 14 GHz, as shown in figure S1 (http://stacks.iop.org/JPhysCM/32/335804/mmedia) in the supporting information. Similar results can also be found in sample A1 (see figure 3(a) in reference [26]) and other two samples (see figure S2 in the supporting information), indicating that pure in-plane UMA exists in the CoFeB films grown on GaAs(001) with the thickness varying from 3.5 nm to 30 nm. By fitting calculations, H_u can be obtained to be 303 Oe, 192 Oe, 113 Oe and 82 Oe for sample A1, A2, A3 and A4, respectively. Figures 3(c) and (d) show the M–H loops for all the samples along the HA and EA, respectively. The H_u value can also be evaluated from the saturation field along the HA, although it can not be determined accurately. From both the FMR and M–H loop measurement results, it can be seen clearly that H_u decreases monotonically with increasing the CoFeB thickness, implying that the UMA is interface induced, which is in agreement with our previous result that H_u is almost inversely proportional to the CoFeB thickness in the range between 3.5 nm and 20 nm [29]. As for the non-monotonic variation of H_c versus the CoFeB film thickness, as shown in figure 3(d), it may be due to the transformation from Néel-type to Bloch-type domain wall with increasing the thickness, which has also been found in FeNi films before [30].

Figure 4(a) shows the fitted H_r–f curves with $\varphi_H = 0°$, 30°, 60°, 90° for sample A2, in which it can be seen clearly that the fitted results (lines) are in good agreement with the experimental ones (dots) and the entire H_r–f curve shifts upwards with rotating H from EA to HA gradually. Similar results can also be seen in other samples, as shown in figure S3 in the supporting information. Besides the resonance field H_r, the linewidth ΔH is another important parameter, which is much correlated to the magnetic damping. Usually, ΔH is analyzed by considering four different contributions given by [7, 17, 18]

$$\Delta H = \Delta H^{Gi} + \Delta H^{2mag} + \Delta H^{mos} + \Delta H^{inh}, \quad (5)$$

where the first and second terms denote the Gilbert and TMS contributions, which are frequency dependent and contribute to magnetic damping certainly. However, because the third term ΔH^{mos} resulted from the orientation spread of the crystallites and the last term ΔH^{inh} caused by the local inhomogeneity are both independent on frequency [7], they do not contribute to magnetic damping. Similar to H_r, the azimuthal dependence of ΔH also demonstrates a twofold symmetry with the minimum (maximum) located at the [110] ([1−10]) direction, as shown in figure 4(b) at f = 10 GHz for sample A2. Similar results can also be found at other frequencies, e.g. 8 GHz and 14 GHz, as shown in figure S4 in the supporting information. In the present FMR measurements, because the microwave driving frequency in the range of (5 GHz, 18 GHz) is much smaller than f_0 ($f_0 = \gamma M_{eff}/2\pi \approx 29.5$ GHz), the frequency dependent

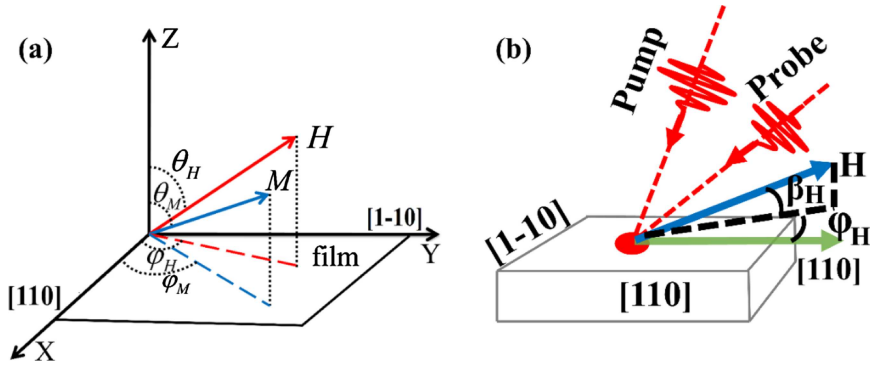

Figure 2. The measurement geometries of VNA-FMR (a) and TRMOKE (b).

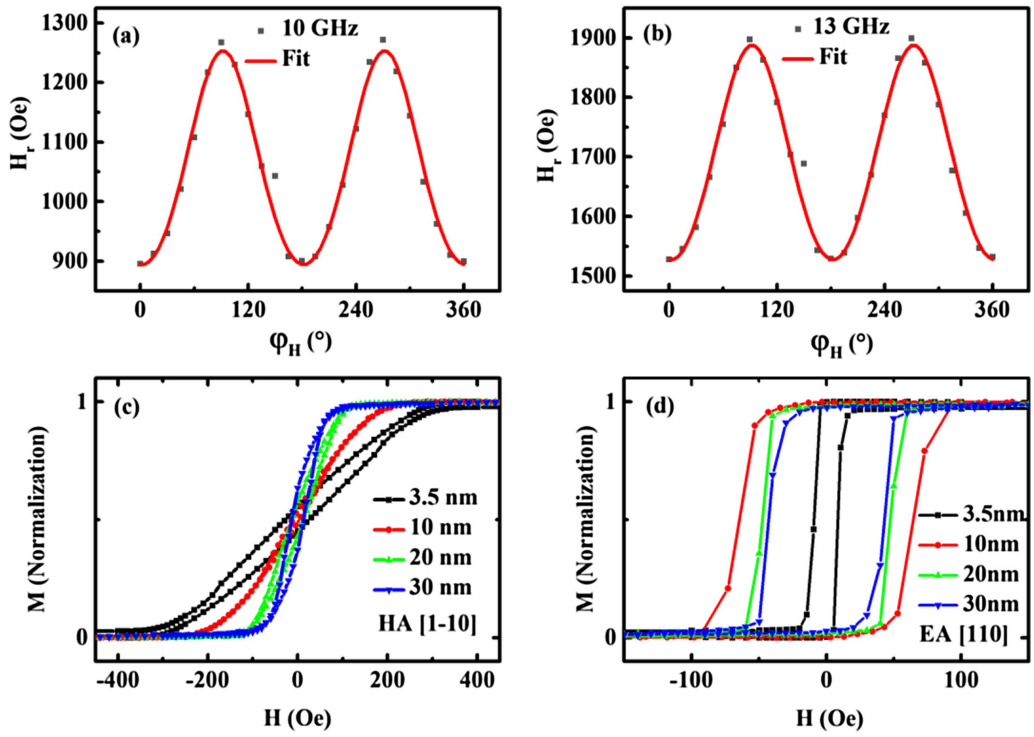

Figure 3. The experimental (square dots) and fitted (red lines) in-plane angular dependent H_r at $f = 10$ GHz (a) and 13 GHz (b) for sample A2. M–H loops along HA (c) and EA (d) for all the samples.

linewidth can be approximately written as [17]

$$\Delta H^{\mathrm{Gi+2mag}} \approx \left[\alpha + \frac{\Gamma_2}{2M_{\mathrm{eff}}}\cos 2(\varphi_{\mathrm{H}} - \varphi_2)\right]\frac{2\pi f}{\gamma} = \alpha_{\mathrm{eff}}\frac{2\pi f}{\gamma}, \tag{6}$$

where α is the Gilbert damping coefficient and considered to be isotropic generally, Γ_2 and φ_2 are induced from the two fold symmetry; α_{eff} is the effective damping coefficient and can be obtained from the slope of a linearly fitted ΔH–f curve.

Figure 4(c) shows that the experimental frequency dependencies of ΔH at $\varphi_{\mathrm{H}} = 0°, 30°, 60°, 90°$ for sample A2, which can be all well fitted in linear functions. Hence, calculated from the slopes, α_{eff} can be obtained to be 0.0116, 0.0124, 0.0192 and 0.0242 when $\varphi_{\mathrm{H}} = 0°, 30°, 60°, 90°$, respectively, which indicates that α_{eff} increases monotonically when the applied field rotates from EA to HA. The linear dependency between ΔH and f at various φ_{H} and the similar variation trend of α_{eff} versus φ_{H} can also be clearly seen in other three samples, as shown in figure S5 in the supporting information. In order to see the in-plane symmetry of α_{eff}, a 360° φ_{H}-scan at every 15° for measuring a ΔH–f curve was performed for sample A2 and the results are displayed in figure 4(d), which can be fairly well fitted according to equation (6). All these above results unambiguously indicate that α_{eff} is anisotropic in the CoFeB films and has the same twofold symmetry as that for H_r or ΔH. In order to compare the damping anisotropy in different samples, a parameter referring to the maximum–minimum ratio is defined by $\eta = \alpha_{\mathrm{eff}}\ (90°)/\alpha_{\mathrm{eff}}\ (0°)$. The calculated values of α_{eff} at $\varphi_{\mathrm{H}} = 0°, 30°, 60°, 90°$ by fitting and the corresponding value of η for all the samples are summarized in table 1. It can be seen that η decreases generally with increasing the CoFeB film thickness, implying that the damping anisotropy is also interface induced, in consistent with the origin

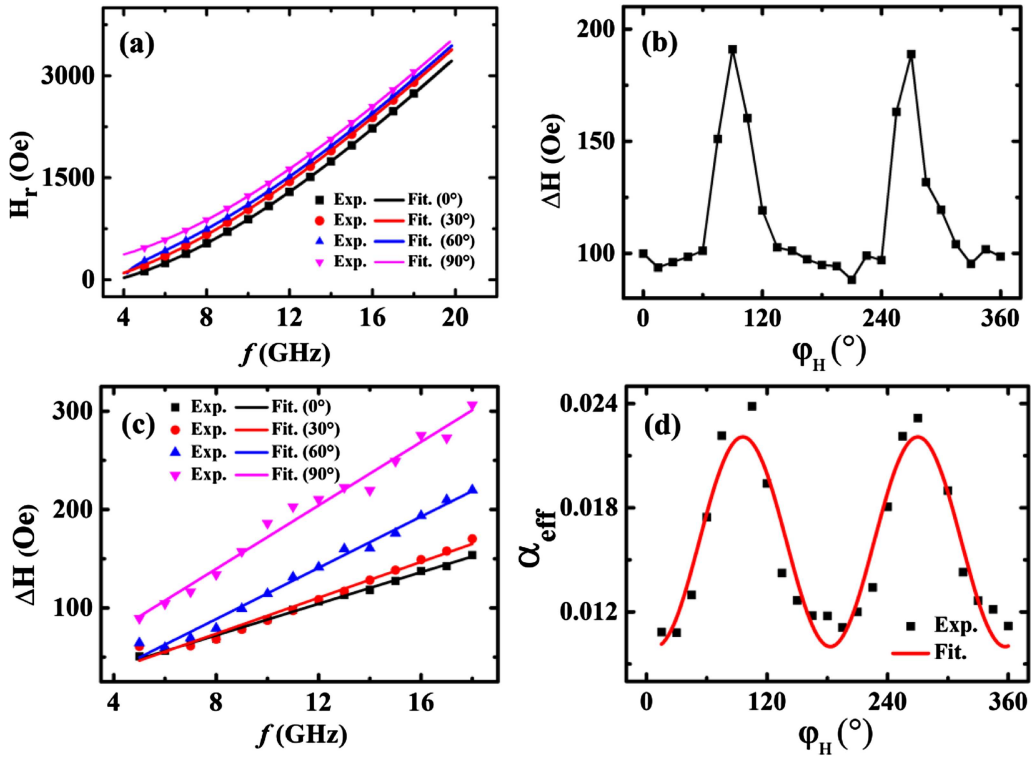

Figure 4. The experimental (dots) and fitted (lines) frequency dependences of H_r with $\varphi_H = 0°$, 30°, 60°, 90° (a), the experimental azimuthal dependence of ΔH (dots) at $f = 10$ GHz (b), the experimental (dots) and fitted (lines) frequency dependences of ΔH with $\varphi_H = 0°$, 30°, 60°, 90° (c), and the experimental (dots) and fitted (line) azimuthal dependences of α_{eff} (d) for sample A2.

Table 1. The angular dependent magnetic damping of samples A1, A2, A3 and A4.

Sample	0°	30°	60°	90°	$\eta = \Delta\alpha/\alpha(0°)$ (%)
A1 (3.5 nm)	0.0140 ± 0.0010	0.0173 ± 0.0008	0.0202 ± 0.0009	0.0260 ± 0.0010	86
A2 (10 nm)	0.0116 ± 0.0003	0.0124 ± 0.0005	0.0192 ± 0.0009	0.0242 ± 0.0009	109
A3 (20 nm)	0.0103 ± 0.0005	0.0104 ± 0.005	0.0141 ± 0.0005	0.0151 ± 0.0005	47
A4 (30 nm)	0.0189 ± 0.0005	0.0193 ± 0.0006	0.0226 ± 0.0007	0.0247 ± 0.0007	31

of UMA as mentioned above. As for the non-monotonic variation of α_{eff} versus the CoFeB film thickness at a fixed φ_H (e.g. 0°), it may be also due to the transformation from Néel-type to Bloch-type domain wall with increasing the FM layer thickness [30].

As discussed above, the anisotropic behavior of α_{eff} in the amorphous CoFeB films can be only generated by two sources, i.e. Gilbert damping and TMS. Since the anisotropy of Gilbert damping can only be observed in some special single-crystalline ferromagnetic thin films [15, 16], it is unlikely to exist in amorphous ferromagnetic films. To our knowledge, the TMS contribution to magnetic damping could be suppressed greatly by increasing the applied magnetic field due to removal of magnon degeneracy [18]. Note that the azimuthal angle of $H(\varphi_H)$ is varied while the out-of-plane angle of $H(\beta_H)$ is fixed at 19° during the TRMOKE measurement. In this way, the anisotropy of α_{eff} can also be characterized by TRMOKE. Figure 5(a) displays several representative precession curves at $\varphi_H = 90°$ for sample A2 when H is increased from 1000 Oe to 13000 Oe. The experimental TRMOKE signal can be analyzed by the following formula [26]

$$\theta_K \sim A + B\exp(-\nu t) + A_0\exp\left(-\frac{t}{\tau}\right)\sin(2\pi ft + \phi_0). \quad (7)$$

Here, A, B and ν are the offset, the background magnitude and the background recovery rate, respectively; A_0, f, τ and ϕ_0 denote precession amplitude, precession frequency, reversal lifetime and initial phase, respectively. As shown in figure 5(a), the experimental TRMOKE results can be well fitted according to equation (7) with removing the second (decaying) term, and the values of f and $1/\tau$ under different H can be obtained consequently. Then, α_{eff} at different H can be calculated by $\alpha_{eff} = 1/2\pi f\tau$ and the results are displayed in figure 5(b), which shows clearly that α_{eff} decreases monotonically with increasing H. Similar to $\varphi_H = 90°$, the monotonic deceases of α_{eff} with increasing H can also be observed at $\varphi_H = 15°$, 30° and 60°. Due to limitation in the measurements, the maximum H can only be applied to be 13 000 Oe. As shown in figure 5(b), although α_{eff} is not fully saturated at $H = 13\,000$ Oe, its reducing speed levels off obviously and the α_{eff} value of 0.0135 obtained at this field must be close to the saturation

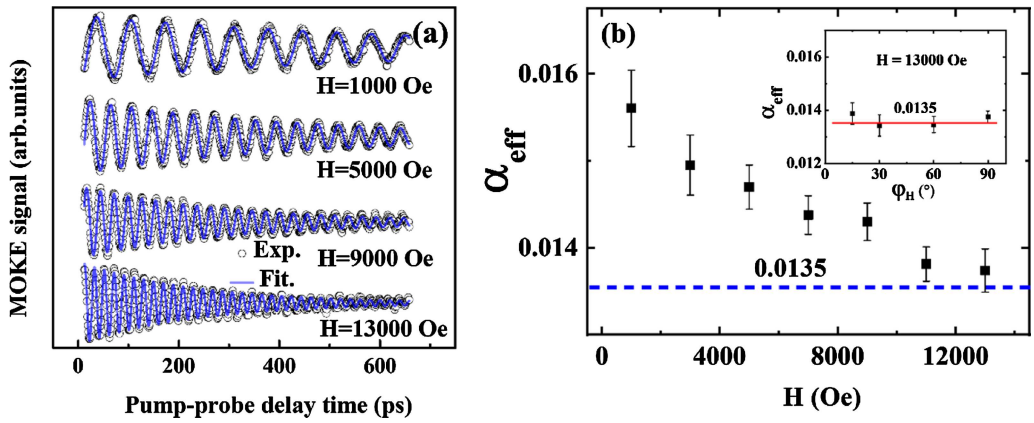

Figure 5. (a) The TRMOKE precession signals obtained under various applied magnetic fields with $\varphi_H = 90°$ and their fits (blue lines) for sample A2. (b) The magnetic field dependence of α_{eff} for sample A2. The inset shows the α_{eff} values at $\varphi_H = 15°$, 30°, 60° and 90° under H = 13 000 Oe. The red line is guide to eyes.

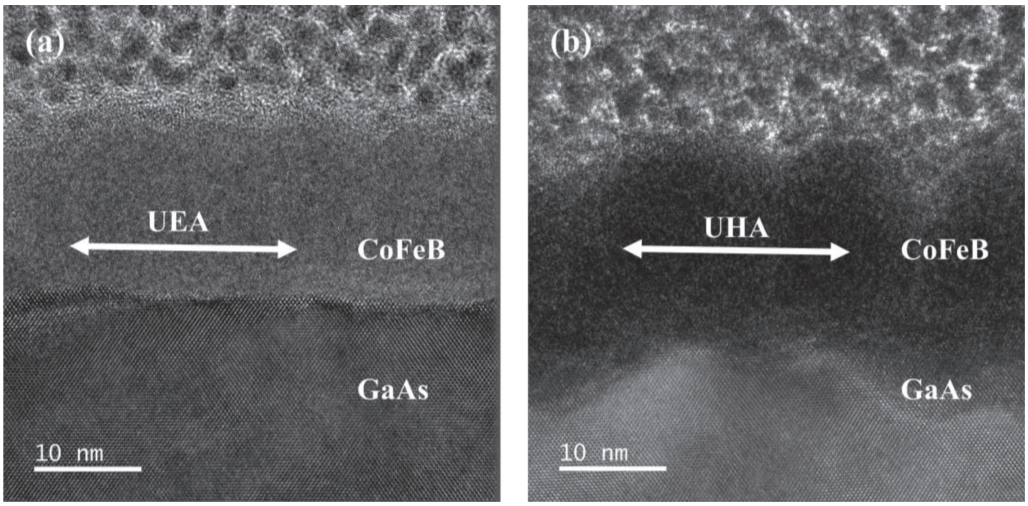

Figure 6. The HRTEM images for sample A2 along the EA (a) and the HA (b) directions.

one. As indicated by the red line in the inset of figure 5(b), α_{eff} holds at about 0.0135 under $H = 13\,000$ Oe at various φ_H, which also supports that the saturation value of α_{eff} under high H is near to 0.0135. Because the TMS contribution to magnetic damping can be greatly suppressed and even removed under high H, it is reasonable to consider that the intrinsic Gilbert damping factor is isotropic (angular independent) in the film plane and approximately to be 0.0135. Therefore, comparing the TRMOKE and VNA-FMR results, it can be concluded that the anisotropy of α_{eff} acquired by VNA-FMR is caused by TMS, while the Gilbert damping is isotropic in the film plane.

It is well accepted that the microscopic mechanism responsible for TMS is originated from surface or interface defects [31, 32]. In order to know the microscopic origins resulting in TMS in the CoFeB films, HRTEM characterizations were performed on sample A2 at the EA and HA directions, and the images are exhibited in figure 6. First, it shows clearly that the CoFeB layer and the Ta capping layer appear to be amorphous because the lattice fringes can hardly be observed. Secondly, comparing figure 6(a) with figure 6(b), the CoFeB–GaAs interface is fairly flat along the EA, while it becomes very rough and meantime serious inter-diffusion happens along the HA. Similar phenomena can be easily observed in other images taken at different places near the CoFeB–GaAs interface. Although the microstructural origin remains unclear, we speculate that reconstruction may happen at the surface of GaAs substrate after pretreatments, which may generate relatively flat and rough surface along [110] and [1−10], respectively. This speculation is consistent with relatively large rms roughness for sample A1 obtained from the AFM image as we reported before [25]. Therefore, after the deposition of the CoFeB film, a significant UMA will be generated with the EA (HA) along [110] ([1−10]) direction. These results are much similar to the generation of UMA in the AlGaAs/GaAs/CoFeB film, in which a kind of corrugation with the lateral period of about 25 nm can be produced at the surface of AlGaAs/GaAs film [23]. Therefore, besides the generation of UMA, the anisotropic CoFeB–GaAs interface can also induce TMS, which is the weakest (strongest) along the EA (HA) and results in anisotropic magnetic damping consequently. Note that the approximate Gilbert damping factor of 0.0135 acquired by TRMOKE is close to but a

little larger than 0.0116 derived from VNA-FMR results along the EA for sample A2. This result supports that the influence of TMS is negligible along the EA, leading to α_{eff} obtained from VNA-FMR close to the Gilbert damping factor. Moreover, the slight increase of Gilbert damping factor acquired by TRMOKE may be ascribed to the heating effect induced by the pump laser excitation during the measurement [33].

4. Conclusions

In summary, the azimuthal dependence of magnetic damping were carefully studied by VNA-FMR in amorphous CoFeB films deposited on GaAs(001) substrates with significant and pure in-plane UMA, and a large anisotropy was observed in the film plane. The anisotropy of effective magnetic damping reduces significantly with increasing the CoFeB film thickness. The TRMOKE technique was also used to characterize the magnetic damping and negligible anisotropy could be observed at high magnetic field. The microstructural analysis reveal that the surface reconstruction of the GaAs(001) substrate may produce the UMA and the TMS as well, which results in the anisotropic magnetic damping. This kind of manipulation of magnetic damping via modifying the interfacial morphology may be a practical way utilized in future magnonic devices.

Acknowledgments

This work was supported by National Key Research and Development Program of China (2016YFA0300803), National Natural Science Foundations of China (Nos. 51971109, 51771053, 51471085), Scientific Research Foundation of Nanjing Institute of Technology (ZKJ201708, CKJB201708).

ORCID iDs

Hongqing Tu https://orcid.org/0000-0003-0117-6684
Zongzhi Zhang https://orcid.org/0000-0003-2032-4929
Jiangtao Qu https://orcid.org/0000-0003-0357-4205
Jun Du https://orcid.org/0000-0002-9967-945X

References

[1] Žutić I, Fabian J and Sarma S D 2004 *Rev. Mod. Phys.* **76** 323–410
[2] Kiselev S I, Sankey J C, Krivorotov I N, Emley N C, Schoelkopf R J, Buhrman R A and Ralph D C 2003 *Nature* **425** 380–3
[3] Lenz K, Wende H, Kuch W, Baberschke K, Nagy K and Jánossy A 2006 *Phys. Rev.* B **73** 144424
[4] Iihama S, Mizukami S, Naganuma H, Oogane M, Ando Y and Miyazaki T 2014 *Phys. Rev.* B **89** 174416
[5] Arias R and Mills D L 1999 *Phys. Rev.* B **60** 7395
[6] Hurben M J and Patton C E 1998 *J. Appl. Phys.* **83** 4344–65
[7] Zakeri K, Lindner J, Barsukov I, Meckenstock R, Farle M, Hörsten U, Wende H, Keune W, Rocker J, Kalarickal S S, Lenz K, Kuch W, Baberschke K and Frait Z 2007 *Phys. Rev.* B **76** 104416
[8] Watanabe H, Kurihara T, Kato T, Yamaguchi K and Suemoto T 2017 *Appl. Phys. Lett.* **111** 092401
[9] Haldar A, Kumar D and Adeyeye A O 2016 *Nat. Nanotechnol.* **11** 437–43
[10] Ando K, Takahashi S, Harii K, Sasage K, Ieda J, Maekawa S and Saitoh E 2008 *Phys. Rev. Lett.* **101** 036601
[11] Liu L Q, Moriyama T, Ralph D C and Buhrman R A 2011 *Phys. Rev. Lett.* **106** 036601
[12] Zhang W, Zhang D, Wong P K J, Yuan H L, Jiang S, Laan G, Zhai Y and Lu Z H 2015 *ACS Appl. Mater. Interfaces* **7** 17070–5
[13] Xue X, Dong G H, Zhou Z Y, Xian D, Hu Z Q, Ren W, Ye Z G, Chen W, Jiang Z D and Liu M 2017 *ACS Appl. Mater. Interfaces* **9** 43188–96
[14] Gilmore K, Stiles M D, Seib J, Steiauf D and Fähnle M 2010 *Phys. Rev.* B **81** 174414
[15] Chen L, Mankovsky S, Wimmer S, Schoen M A W, Körner H S, Kronseder M, Schuh D, Bougeard D, Ebert H, Weiss D and Back C H 2018 *Nat. Phys.* **14** 490–4
[16] Li Y, Zeng F L, Zhang S S L, Shin H, Saglam H, Karakas V, Ozatay O, Pearson J E, Heinonen O G, Wu Y Z, Hoffmann A and Zhang W 2019 *Phys. Rev. Lett.* **122** 117203
[17] Belmeguenai M, Tuzcuoglu H, Gabor M S, Petrisor T, Tiusan C, Berling D, Zighem F, Chauveau T, Chérif S M and Moch P 2013 *Phys. Rev.* B **87** 184431
[18] Qiao S, Yan W, Nie S H, Zhao J H and Zhang X H 2015 *AIP Advances* **5** 087170
[19] Chen Z D, Kong W W, Mi K, Chen G L, Zhang P, Fan X L, Gao C X and Xue D S 2018 *Appl. Phys. Lett.* **112** 122406
[20] Kasatani Y, Yamada S, Itoh H, Miyao M, Hamaya K and Nozaki Y 2014 *Appl. Phys. Express* **7** 123001
[21] Yilgin R, Sakuraba Y, Oogane M, Mizukami S, Ando Y and Miyazaki T 2007 *Jpn. App. Phys.* **46** L205–8
[22] Li Y, Li Y, Liu Q, Yuan Z, Zhan Q F, He W, Liu H L, Xia K, Yu W, Zhang X Q and Cheng Z H 2019 *New J. Phys.* **21** 123001
[23] Hindmarch A T, Kinane C J, MacKenzie M, Chapman J N, Henini M, Taylor D, Arena D A and Dvorak J 2008 *Phys. Rev. Lett.* **100** 117201
[24] Hindmarch A T, Rushforth A W, Campion R P, Marrows C H and Gallagher B L 2011 *Phys. Rev.* B **83** 212 404
[25] Tu H Q, You B, Zhang Y Q, Gao Y, Xu Y B and Du J 2015 *IEEE Trans. Magn.* **51** 2002104
[26] Tu H Q, Liu B, Huang D W, Ruan X Z, You B, Huang Z C, Zhai Y, Gao Y, Wang J, Wei L J, Yuan Y, Xu Y B and Du J 2017 *Sci. Rep.* **7** 43971
[27] Qiao S, Nie S H, Zhao J H, Huo Y, Wu Y Z and Zhang X H 2013 *Appl. Phys. Lett.* **103** 152402
[28] Iihama S, Ma Q L, Kubota T, Mizukami S, Ando Y and Miyazaki T 2012 *Appl. Phys. Express* **5** 083001
[29] Tu H Q, You B, Gao Y, Wang J, Ruan X Z and Du J 2016 *J. Supercond. Nov. Magn.* **29** 2843–8
[30] Chen Y C, Hung D S, Yao Y D, Lee S F, Ji H P and Yu C 2007 *J. Appl. Phys.* **101** 09C104
[31] Lindner J, Lenz K, Kosubek E, Baberschke K, Spoddig D, Meckenstock R, Pelzl J, Frait Z and Mills D L 2003 *Phys. Rev.* B **68** 060102
[32] Körner M, Lenz K, Gallardo R A, Fritzsche M, Müchlich A, Facsko S, Lindner J, Landeros P and Fassbender J 2013 *Phys. Rev.* B **88** 054405
[33] Liu B, Ruan X Z, Wu Z Y, Tu H Q, Du J, Wu J, Lu X Y, He L, Zhang R and Xu Y B 2016 *Appl. Phys. Lett.* **109** 042401